Fast-neutron activation of long-lived isotopes in enriched Ge

S. R. Elliott,[*] V. E. Guiseppe,[†] and B. H. LaRoque

Physics Division, Los Alamos National Laboratory, Los Alamos, New Mexico 87545, USA

R. A. Johnson

Department of Physics, University of Washington, Seattle Washington, 98195, USA

S. G. Mashnik

XCP Division, Los Alamos National Laboratory, Los Alamos, New Mexico 87545, USA

We measured the production of ^{57}Co, ^{54}Mn, ^{68}Ge, ^{65}Zn, and ^{60}Co in a sample of Ge enriched in isotope 76 due to high-energy neutron interactions. These isotopes, especially ^{68}Ge, are critical in understanding background in Ge detectors used for double β decay experiments. They are produced by cosmogenic-neutron interactions in the detectors while they reside on the Earth's surface. These production rates were measured at neutron energies of a few hundred MeV. We compared the measured production to that predicted by cross-section calculations based on CEM03.02. The cross-section calculations overpredict our measurements by approximately a factor of 3 depending on isotope. We then use the measured cosmic-ray neutron flux, our measurements, and the CEM03.02 cross sections to predict the cosmogenic production rate of these isotopes. The uncertainty in extrapolating the cross-section model to higher energies dominates the total uncertainty in the cosmogenic production rate.

I. INTRODUCTION

Neutrinoless double β decay ($0\nu\beta\beta$) plays a key role in understanding the neutrino's absolute mass scale and particle-antiparticle nature [1–6]. If this nuclear decay process exists, one would observe a monoenergetic line originating from a material containing an isotope subject to this decay mode. One such isotope that may undergo this decay is ^{76}Ge. Germanium-diode detectors fabricated from material enriched in ^{76}Ge have established the best half-life limits and the most restrictive constraints on the effective Majorana mass for the neutrino [7,8]. One analysis [9] of the data in Ref. [8] claims evidence for the decay with a half-life of $2.23^{+0.44}_{-0.31} \times 10^{25}$ y. Planned Ge-based $0\nu\beta\beta$ experiments, MAJORANA [10–12] and GERDA [13], will test this claim. Eventually, these future experiments target a sensitivity of $>10^{27}$ y or $\sim$1 event/ton-year to explore neutrino mass values near that indicated by the atmospheric neutrino oscillation results.

The key to these experiments lies in the ability to reduce intrinsic radioactive background to unprecedented levels and to adequately shield the detectors from external sources of radioactivity. Previous experiments' limiting backgrounds have been trace levels of natural decay chain isotopes within the detector and shielding components. The γ-ray emissions from these isotopes can deposit energy in the Ge detectors producing a continuum, which may overwhelm the potential $0\nu\beta\beta$ signal peak at 2039 keV. Great progress has been made in identifying the location and origin of this contamination, and future efforts will substantially reduce this contribution to the

background. The background level goal of 1 event/ton-year, however, is an ambitious factor of $\sim$400 improvement over the currently best achieved background level [8]. If the efforts to reduce the natural decay chain isotopes are successful, previously unimportant components of the background must be understood and eliminated. The contribution from long-lived isotopes produced by cosmic-ray neutrons in Ge detectors fabricated from enriched Ge was recognized and described in Refs. [14,15]. In fact, the dominant background that the MAJORANA and GERDA experiments will face, without sophisticated analysis cuts, will originate from such isotopes unless mitigation strategies to reduce the activation are successful.

To successfully mitigate the impact of these isotopes requires an understanding of their production. Tables I and II summarize the previous production rate estimates. The two most critical cosmogenic isotopes, ^{60}Co and especially ^{68}Ge, show significant variation in the predicted rates: factors of $\approx$2 and $\approx$10 respectively. For ^{60}Co, some models predict a higher production rate for enriched Ge ($^{\mathrm{enr}}$Ge) than for Ge samples with natural isotopic content ($^{\mathrm{nat}}$Ge). Reference [16] gives a nice summary of previous attempts to calculate the production rates of the problematic isotopes, and provides an estimate of its own. The authors of that report noted that the calculations differ significantly and that measurements would be useful to better understand the rates. Some measurements do exist but are either for proton reactions [17–19] or have a large uncertainty [15]. Since the production rates due to neutrons are much larger than for protons, it is important to have neutron reaction measurements. In addition, Barabanov *et al.* [20] studied the reduction of cosmogenic activation as it depends on shielding in order to design an optimum transport container. That reference also calculated the rates for cosmic-ray proton reactions and found the production rates for the troublesome isotopes to be about a factor of 10 below that

---

[*]elliotts@lanl.gov

[†]Present address: University of South Dakota, Vermillion, SD 57069.

TABLE I. A summary of previous estimates of the production of long-lived cosmogenic isotopes in ^{nat}Ge for the isotopes studied in this work. The production rates are given in atoms per kg d. The data in Ref. [27] was quoted in μBq/kg and we converted to units presented.

Isotope	Ref. [14]	Ref. [15] (Calc.)	Ref. [15] (Expt.)	Ref. [27]	Ref. [20]	Ref. [16]	Ref. [23]	Ref. [21]
^{57}Co	0.5	4.4	2.9 ± 0.4	10.2		9.7	6.7	13.5
^{54}Mn		2.7	3.3 ± 0.8	9.1		7.2		2.7
^{68}Ge	26.5	29.6	30 ± 7	58.4	82.8	89	45.8	41.3
^{65}Zn	30.0	34.4	38 ± 6	79.0		77	29.0	37.1
^{60}Co	4.8			6.6	2.9	4.8	2.8	2.0

for cosmic-ray neutrons. The work of Mei *et al.* [21] noted that much of the large variation in these rates was due to the use of different cosmic ray neutron flux estimates and that many of the analyses [14,15,20,22,23] used historical flux spectra that are less precise than modern measurements. Although Ref. [21] performed calculations for the production of the isotopes of interest to this article, the cross sections were calculated using TALYS [24]. This code only predicts cross sections to an energy of 250 MeV, whereas other treatments go to higher energies. Reference [16] used a modern interpretation of the old neutron flux values [25] but not the results of recent measurements [26]. Furthermore, it used a combination of cross-section calculations in order to span the energies necessary for the calculations. Reference [27] presented numbers for a specific shielding geometry, which is not easy to translate to a raw production rate with the provided data. Hence none of the presently available estimates are sufficient to reliably predict the cosmogenic production rates and new measurements and estimates are required.

We exposed a sample of Ge enriched in isotope 76 to a wide-band neutron beam that resembles the cosmic-ray neutron flux. After exposure we counted the sample in a low-background counting system to observe the γ rays from the decays of the problematic isotopes. From these data we have measured the production rate due to fast neutrons in a Ge sample enriched in isotope 76 that was taken from material used for Ge detector production. With knowledge of the neutron-beam and cosmic-neutron energy spectra, we

TABLE II. A summary of previous estimates of the production of long-live cosmogenic isotopes in ^{enr}Ge for the isotopes studied in this work. For these estimates, the abundance values are 14% for ^{74}Ge, 86% for ^{76}Ge, and zero for the other naturally occurring isotopes. The production rates are given in atoms per kg d.

Isotope	Ref. [14]	Ref. [15]	Ref. [22]	Ref. [20]	Ref. [16]	Ref. [23]	Ref. [21]	This work
^{57}Co	0.1	1.0	1.6		2.3	2.9	6.7	0.7 ± 0.4
^{54}Mn		1.4	2.3		5.4	2.2	0.87	2.0 ± 1.0
^{68}Ge	1.2	1.2		5.7	13	7.6	7.2	2.1 ± 0.4
^{65}Zn	6.0	6.4	11.0		24	10.4	20.0	8.9 ± 2.5
^{60}Co	3.5			3.3	6.7	2.4	1.6	2.5 ± 1.2

used these data to provide an estimate of the production rate due to exposure of Ge to cosmic rays. We used a cross-section calculation that spans the energy range of interest and the most recent cosmic-ray neutron flux measurements of which we are aware. This article describes our determination of values for the production rate of these isotopes.

II. EXPERIMENT

The sample was exposed to the neutron beam at the Los Alamos Neutron Science Center (LANSCE) Weapons Neutron Research (WNR) facility from Target 4 Flight Path 60 Right (4FP60R) [28]. As the broad-spectrum, pulsed neutron beam strikes the Ge target, the outgoing γ rays are detected by the Germanium Array for Neutron Induced Excitations (GEANIE) spectrometer [29]. The corresponding data from the GEANIE spectrometer will be used for $(n, n'\gamma)$ analysis that will be presented in a separate publication. The GEANIE sample is located a distance of 20.34 m from the natural tungsten spallation target.

The target sample was a 11.13-gm, 22-mm diameter metal enriched Ge (^{enr}Ge) powder contained within a plastic enclosure. The isotopic abundances within the sample were measured by time-of-flight secondary ion mass spectrometry (ToF SIMS) with the result: ^{70}Ge $0.77 \pm 0.04\%$, ^{72}Ge $0.94 \pm 0.05\%$, ^{73}Ge $0.36 \pm 0.03\%$, ^{74}Ge $13.81 \pm 0.18\%$, and ^{76}Ge $84.12 \pm 0.23\%$. The sample was exposed with two separate beam collimations ($3/4''$ and $1/2''$ collimators) during three irradiation periods. For the $3/4''$-collimator ($1/2''$-collimator) run a surface area of 2.85 (1.27) cm^2 was exposed to the beam. The $3/4''$-collimator exposure was performed between July 16 and July 23, 2007 (6.99 d elapsed time). The $1/2''$-collimator exposure was performed between July 27 and August 2, 2007 (5.95 d) and then between August 8 and August 14, 2007 (6.19 d). As seen in Fig. 1, the energy spectrum of the third exposure was slightly softer than the other two exposures at the higher energies. The pulsed neutron beam has the following timing structure. Macropulses, lasting 625 μs, occur at a rate of 40 Hz. Micropulses are spaced every 1.8 μs, during which the neutron energy is determined by the time of flight from the micropulse start. An in-beam fission chamber measures the neutron flux with ^{238}U foils. If the reader wishes to convolve the neutron spectrum with his/her own cross-section model,
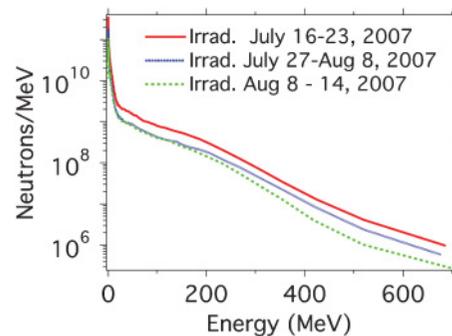
FIG. 1. (Color online) The energy spectrum for the neutron beam fluence at 4FP60R for the three separate exposure periods. The data are corrected for live time of the fission chamber.
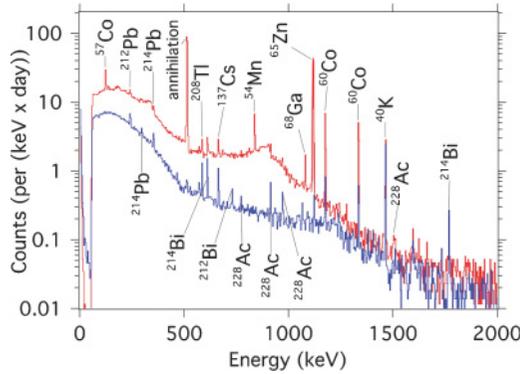
FIG. 2. (Color online) The energy spectrum of γ rays from the $^{\mathrm{enr}}$Ge sample as measured by a Ge detector (upper curve). Also shown is a background spectrum taken with no sample present. (lower curve)

we give a parametrization of the neutron spectrum impinging on our sample for convenience. The spectrum can be described as:

$$\Phi(E) = (1.325 \times 10^{-10})$$
$$\times e^{(4.986 \ln E - 3.825 \ln^2 E + 0.9159 \ln^3 E - 0.07402 \ln^4 E)}, \quad (1)$$

where Φ is in units of neutrons/MeV and the energy (E) is in MeV.

The powder was stored for an extended period and therefore any radioactivity had decayed to an extremely low level (<150 Bq) before counting began. Therefore, this sample was well below any action levels and not subject to any source-handling requirements. The sample was transported to our low-background counting facility underground at the Waste Isolation Pilot Plant (WIPP) near Carlsbad (New Mexico) and counted with a Ge detector. The detector was fabricated in 1985 and placed underground at WIPP in 1998. It is an n-type semicoax design with a height of 41 mm and a diameter of 51 mm. It is contained within an ≈ 1-mm-thick Cu cryostat. The shield during these runs consisted of 5 cm of oxygen-free, high-conductivity Cu and 10 cm of Pb.

The sample was counted over a period of 73.86 days between February 19 and May 4, 2009, with a total live time of 49.02 days. The spectrum is shown in Fig. 2. The detector at WIPP has been underground there for over 10 years and therefore any activities of isotopes of interest to this study,

that may have been produced while that detector was exposed to cosmic rays as it resided on the Earth's surface, have long since decayed away. The lone exception to this is a very low level of ^{60}Co that resides in the Cu cryostat of the Ge detector and the inner layer of the shield that is also Cu. The background spectrum in Fig. 2 shows that this rate is very small compared to the sample's ^{60}Co rate. The data presented in Table III includes a subtraction of this background ($\approx 10\%$) for the ^{60}Co count rates.

III. MEASURED PRODUCTION RATES

The peaks in Fig. 2 were fit to determine the measured counts (C) and the results are given in Table III. The efficiency for counting the γ rays in the geometry used for the sample was determined by using ^{57,60}Co, ^{54}Mn, ^{22}Na, and ^{137}Cs sources. The geometry of these sources is coincidently very similar to the Ge sample and therefore there was no need for simulation to determine the efficiencies. These sources had calibrated activities known to $\pm 1\%$. Since many of the lines of interest come from these isotopes, the measurements were a direct calibration of the efficiencies of interest. For ^{65}Zn and ^{68}Ga lines, a γ-ray efficiency curve was determined from the various lines in these sources in order to interpolate between the measured line energies. Corrections for summing of coincident transitions and annihilation γ rays within the sources were made. The resulting efficiencies and their uncertainty resulting from counting statistics and the interpolation and summing corrections are given in Table III. For the ^{60}Co calibration, a high event rate resulted in a minor peak distortion that the other data sets did not suffer. We took an additional uncertainty for those peaks to reflect that. We used a random pulser to verify the event-rate dependence of the data-acquisition system dead time.

In addition to the γ-ray detection efficiency (ϵ_γ), an efficiency factor must also be included to take into account the decay of the isotope since the end of exposure and during the counting period. This latter efficiency factor (ϵ_c) depends on the half-life of the isotope of interest and is also given in Table III.

With these efficiencies, it is straightforward to calculate the number of atoms of each isotope that were present at the end of exposure to neutrons (August 14, 2007). The measured number of atoms at the reference date of the end of exposure

TABLE III. A summary of N_0 for the long-lived isotopes in the $^{\mathrm{enr}}$Ge sample. The uncertainty quoted for N_0 is statistical and arises only from the counting statistics of the measured peaks. The quoted uncertainty for N_0^{Pred} arises from the uncertainty in the 4FP60R neutron fluence. Systematic uncertainties are summarized in Table XI and discussed in the text.

Isotope	$\tau_{1/2}$ (days)	γ-ray energy (keV)	C	ϵ_γ	ϵ_c	B	N_0	N_0^{Pred}
^{57}Co	271.8	122.1	2916 ± 84	0.1663(7)	0.0280	0.856	$(7.31 \pm 0.21) \times 10^5$	$(2.97 \pm 0.06) \times 10^6$
^{57}Co	271.8	136.5	386 ± 63	0.163(2)	0.0280	0.107	$(7.89 \pm 1.3) \times 10^5$	$(2.97 \pm 0.06) \times 10^6$
^{54}Mn	312.1	834.9	1084 ± 43	0.0302(3)	0.0297	1.000	$(1.21 \pm 0.05) \times 10^6$	$(1.79 \pm 0.05) \times 10^6$
^{68}Ge	270.8	1077.4	198 ± 18	0.0207(5)	0.0280	0.032	$(1.06 \pm 0.10) \times 10^7$	$(2.92 \pm 0.02) \times 10^7$
^{65}Zn	244.25	1115.5	8541 ± 95	0.0232(5)	0.0262	0.506	$(2.77 \pm 0.03) \times 10^7$	$(5.03 \pm 0.06) \times 10^7$
^{60}Co	1923.6	1173.2	1342 ± 42	0.0200(6)	0.0146	0.999	$(4.61 \pm 0.14) \times 10^6$	$(7.50 \pm 0.01) \times 10^6$
^{60}Co	1923.6	1332.5	1176 ± 39	0.0167(3)	0.0146	1.000	$(4.83 \pm 0.16) \times 10^6$	$(7.50 \pm 0.01) \times 10^6$

(N_0) is given by

$$N_0 = \frac{C}{\epsilon_\gamma \epsilon_c B},\qquad(2)$$

where

$$\epsilon_c = \sum_i \left(e^{-\lambda T^i_{\text{start}}} - e^{-\lambda T^i_{\text{end}}}\right),\qquad(3)$$

and T^i_{end} (T^i_{start}) is the number of days since the end of exposure that the counting stopped (started) for each of the i data runs, λ is the decay rate of the isotope in question, and B is the fraction of decays that emit the γ ray of interest.

The predicted number of atoms N_0^{Pred} can also be expressed in terms of the reaction rates during the three exposure periods:

$$N_0^{\text{Pred}} = \sum_i \frac{k_i}{\lambda}\left(1 - e^{-\lambda T^i_{\text{irrad}}}\right)e^{-\lambda T^i_{\text{decay}}},\qquad(4)$$

where we have corrected for the decay during the exposure and the decay after the exposure until the reference date. In Eq. (4), T^i_{irrad} is the duration time of irradiation of the ith exposure, and T^i_{decay} is the time between the end of exposure i and the reference date for N_0. k_i is the production rate (atoms per day) during exposure i and is given by:

$$k_i = \frac{n_s}{t_i}\int F_i(E)\sigma(E)dE = \left[\frac{M_s N_A}{(MW)At_i}\right]f_i,\qquad(5)$$

where n_s is the number of exposed sample nuclei per unit area in exposure i of duration t_i, $F_i(E)$ is the energy-(E) dependent neutron fluence (number of neutrons per MeV) impinging on the sample during exposure i, and $\sigma(E)$ is the energy-dependent cross section calculated for our sample and its measured isotopic abundances. f_i is the fluence and cross-section energy-dependent integral for each exposure. The areal density, n_s, is related to the total sample mass (M_s, 11.13 g) and the sample area (A, 3.80 cm^2). The beam spot covers most, but not all, of the sample geometry and therefore we have ignored any uncertainty associated with nonuniformities in the powdered sample thickness. That is, any such nonuniformities will average to the nominal areal density.

N_0^{Pred} can be written:

$$N_0^{\text{Pred}} = \frac{M_s N_A}{(MW)\lambda A}\sum_i f_i\left(1 - e^{-\lambda T^i_{\text{irrad}}}\right)e^{-\lambda T^i_{\text{decay}}},\qquad(6)$$

where N_A is Avagadro's number and MW is the molecular weight (75.62 u for our sample).

A number of systematic effects add to the uncertainty in N_0. These include the uncertainty in the nuclear physics parameters, which come from the National Nuclear Data Center. The values for the half-lives and branching ratios are known to high precision and are a negligible contribution to the total uncertainty. The uncertainly in ϵ_γ is described above and included in the quoted values. However, each of the sources have an additional uncertainty due to the precision of the known activity of 1%. The start and stop times of counting and the live time of the counting are known to a small percentage and are negligible contributions to the uncertainty. This is similar for the times associated with the irradiation. The

sample had been stored on the Earth's surface for many years prior to exposure to the beam and then counting at WIPP. Any isotopes produced by cosmic ray neutrons would certainly be at saturation after this extended period. The saturation production rates, however, are predicted to be near 1 atom/(d kg). Therefore the total count rate for our 11-g sample due to this contribution is several orders of magnitude less than our measured count rate and we ignore this systematic effect.

One can assign an effective energy at which these measurements were made as that for which the theoretical production rate (the product of the CEM cross section and the 4FP60R flux) peaks. Table IX provides the effective energy for each of the isotopes in question. The measured uncertainty in the production rates at these energies are given in Table XI in the *subtotal* column.

IV. CROSS SECTIONS

If the energy dependence of the neutron fluence over the duration of the exposure had been constant and identical in shape to the cosmic-ray neutron flux, we could have used a simple neutron-flux scaling between our measurements and the cosmic-neutron flux to estimate the cosmogenic production of these isotopes. Since the shapes do differ, we used a model for the cross section to adjust for these spectral differences in order to make a prediction regarding the cosmic-ray production rates. For this purpose, we use cross sections for isotope production calculated using cascade-exciton model (CEM03.02 [30–32]) as it usually has a better predictive power in comparison with other similar available models (see, e.g., Ref. [33]). The CEM formalism permits the calculation of cross sections to the high energies necessary for this work. We assumed that the energy dependence of the cross section is nearly correct but that there may be an overall normalization uncertainty. This procedure then corrects for any normalization uncertainty. Below we describe how we estimate the uncertainty associated with the energy-dependence assumption.

To determine the yield of an isotope, one must consider all feeder isotopes that may decay to the isotope of interest. Therefore to determine the cumulative cross section for ^{57}Co for example, one must sum the cross sections for ^{57}Co, ^{57}Ni, ^{57}Cu, and ^{57}Zn. Similarly for ^{68}Ge, one must also consider ^{68}As and for ^{65}Zn one must consider ^{65}Zn, ^{65}Ga, ^{65}Ge, and ^{65}As. For the isotopes ^{54}Mn and ^{60}Co one only need consider the primary isotopes. Note that for the case of ^{60}Co, this is only approximately true. Because of the long half-life of ^{60}Fe, the contributions of ^{60}Fe, ^{60}Mn, and ^{60}Cr are negligible. Using the CEM3.02 code, Tables IV through VIII provide the values of these cumulative cross sections summed over the feeders for the five isotopes that comprise Ge.

Table IX gives the critical neutron energy range for the majority of the isotope production rate. This low (high) value of this energy range is defined as the energy for which 10% (90)% of the cumulative production rate is reached. The ranges are given for both the 4FP60R beam spectrum and the cosmic ray flux. The 4FP60R range also is calculated for the isotopic abundance of our sample, whereas the cosmic ray flux column is calculated for our standard 86–14% isotopic enrichment. Although the energy at which the peak of the production rate

TABLE IV. The calculated cumulative cross sections for production of selected cosmogenic isotopes in ^{70}Ge. The cross sections are cumulative because they are sums over all isotopes that feed the isotope of interest.

Energy (MeV)	Isotope production cross section (mb)				
	^{57}Co	^{54}Mn	^{68}Ge	^{65}Zn	^{60}Co
10	0	0	0	0	0
20	0	0	0	0	0
30	0	0	295.6	16.63	0
40	0	0	248.0	97.52	0
50	0	0	153.1	51.05	0.0022
60	0	0	119.6	36.86	0.034
70	0	0	101.6	55.99	0.53
80	0.009	0.001	90.53	86.66	0.80
90	0.019	0.0019	82.67	91.14	0.70
100	0.16	0.0037	75.15	88.94	0.80
200	11.49	3.06	50.42	54.34	4.78
300	16.52	7.72	43.50	47.17	4.34
400	18.97	10.59	38.13	41.63	4.38
500	20.34	12.86	33.34	37.14	4.36
600	20.28	14.31	29.17	33.39	4.21
700	19.09	14.49	26.46	30.89	3.81
800	18.59	14.15	24.75	28.58	3.63
900	17.28	13.59	23.36	27.026	3.34
1000	16.27	13.08	22.07	25.99	3.11
2000	10.22	8.12	16.62	20.61	2.17

TABLE VI. The calculated cumulative cross sections for production of selected cosmogenic isotopes in ^{73}Ge. The cross sections are cumulative because they are sums over all isotopes that feed the isotope of interest.

Energy (MeV)	Isotope production cross section (mb)				
	^{57}Co	^{54}Mn	^{68}Ge	^{65}Zn	^{60}Co
10	0	0	0	0	0
20	0	0	0	0	0
30	0	0	0	0	0
40	0	0	0	0	0
50	0	0	0	0	0
60	0	0	4.79	0.08	0
70	0	0	22.14	6.67	0
80	0	0	23.51	13.28	0.002
90	0	0	19.93	11.61	0.017
100	0	0	18.37	12.60	0.13
200	3.63	0.52	15.22	35.05	4.94
300	7.45	3.87	14.00	33.30	6.14
400	10.40	7.34	11.98	30.62	6.88
500	12.84	10.60	10.39	27.92	7.32
600	14.07	13.07	9.20	25.63	7.37
700	13.83	14.45	8.41	23.38	7.17
800	13.67	14.57	7.84	21.48	6.91
900	13.06	14.49	7.25	19.88	6.51
1000	12.51	13.81	6.92	18.58	6.19
2000	7.73	8.64	5.53	12.96	3.94

TABLE V. The calculated cumulative cross sections for production of selected cosmogenic isotopes in ^{72}Ge. The cross sections are cumulative because they are sums over all isotopes that feed the isotope of interest.

Energy (MeV)	Isotope production cross section (mb)				
	^{57}Co	^{54}Mn	^{68}Ge	^{65}Zn	^{60}Co
10	0	0	0	0	0
20	0	0	0	0	0
30	0	0	0	0	0
40	0	0	0	0	0
50	0	0	15.82	0.15	0
60	0	0	45.86	13.43	0
70	0	0	42.57	20.87	0.0010
80	0	0	34.56	18.01	0.014
90	0	0	32.2	19.43	0.20
100	0	0	30.69	30.27	0.61
200	4.32	0.99	22.9	42.50	5.26
300	10.00	5.03	19.88	38.31	5.78
400	12.86	8.55	16.91	34.84	6.22
500	15.12	11.47	14.77	31.37	6.56
600	16.05	13.91	13.46	28.30	6.45
700	15.95	14.48	12.45	25.54	6.09
800	15.22	14.62	11.54	23.63	5.85
900	14.37	14.54	11.13	21.75	5.52
1000	13.45	14.07	10.65	20.59	5.14
2000	8.24	8.79	7.96	14.69	3.27

TABLE VII. The calculated cumulative cross sections for production of selected cosmogenic isotopes in ^{74}Ge. The cross sections are cumulative because they are sums over all isotopes that feed the isotope of interest.

Energy (MeV)	Isotope production cross section (mb)				
	^{57}Co	^{54}Mn	^{68}Ge	^{65}Zn	^{60}Co
10	0.00	0.00	0.00	0.00	0.00
20	0.00	0.00	0.00	0.00	0.00
30	0.00	0.00	0.00	0.00	0.00
40	0.00	0.00	0.00	0.00	0.00
50	0.00	0.00	0.00	0.00	0.00
60	0.00	0.00	0.00	0.00	0.00
70	0.00	0.00	0.57	0.00	0.00
80	0.00	0.00	7.78	1.61	0.00
90	0.00	0.00	13.04	6.79	0.00
100	0.00	0.00	12.79	8.06	0.01
200	1.03	0.23	10.76	28.71	4.07
300	5.37	2.73	10.43	28.24	6.04
400	8.16	6.14	8.74	27.13	7.28
500	10.85	9.52	7.69	25.33	8.09
600	12.16	12.18	6.85	23.42	8.08
700	12.77	13.66	6.17	21.17	8.19
800	12.40	14.34	5.44	19.32	7.64
900	11.96	14.44	5.11	17.64	7.32
1000	11.36	13.93	4.78	16.47	6.88
2000	7.03	8.76	3.79	11.31	4.46

TABLE VIII. The calculated cumulative cross sections for production of selected cosmogenic isotopes in ^{76}Ge. The cross sections are cumulative because they are sums over all isotopes that feed the isotope of interest.

Energy	Isotope production cross section (mb)				
(MeV)	^{57}Co	^{54}Mn	^{68}Ge	^{65}Zn	^{60}Co
10	0.00	0.00	0.00	0.00	0.00
20	0.00	0.00	0.00	0.00	0.00
30	0.00	0.00	0.00	0.00	0.00
40	0.00	0.00	0.00	0.00	0.00
50	0.00	0.00	0.00	0.00	0.00
60	0.00	0.00	0.00	0.00	0.00
70	0.00	0.00	0.00	0.00	0.00
80	0.00	0.00	0.00	0.00	0.00
90	0.00	0.00	0.04	0.00	0.00
100	0.00	0.00	1.00	0.19	0.00
200	0.12	0.11	5.52	17.18	1.95
300	2.43	1.24	5.92	19.91	5.07
400	4.92	3.94	5.27	20.67	7.15
500	7.39	7.15	4.69	20.14	8.52
600	9.16	10.34	4.11	18.97	9.12
700	9.84	12.25	3.73	17.41	9.40
800	10.21	13.63	3.36	16.11	9.16
900	10.02	13.86	3.08	14.84	8.66
1000	9.62	14.00	2.85	13.60	8.36
2000	5.82	8.92	1.82	8.67	5.43

FIG. 3. The CEM cross sections folded with the cosmic-ray neutron energy spectrum as a function of energy for the isotopes of interest.

variation in the cross-section uncertainty with energy to be large. References [30–34] indicate that the predictions of the model are uniform across that range. Reference [33] presents a quantitative analysis of the comparison between the model and previous experiments using a large number of data sets. The result is that the uncertainty is fairly energy independent with a 2–10% change depending on the data set used for comparison.

Unfortunately there is a lack of cross-section data for large ΔA transitions induced by fast neutrons. Such data would directly validate the theoretical model for interpreting our production rate measurements in terms of the cosmic-ray neutron flux. Reference [33], however, provides data on proton-induced transitions on an ^{56}Fe target with ΔA values similar to those of interest in this work. (See Figs. 3–5 in that work.) For each isotope considered here, we use the data of Ref. [33] to estimate the uncertainty that may arise from the energy dependence of the cross section.

The critical energy range for the cosmic-ray production rate for the most important $\beta\beta$-background isotope, ^{68}Ge, is between 110 and 530 MeV. [The low (high) energy of this range was defined by integrating over energy up to the 10% (90%) value of the total production rate.] Reference [33] studied a few $\Delta A = 8$ transitions in ^{56}Fe (similar to the production of ^{68}Ge from ^{76}Ge) that can be used to estimate this

for the two spectra are similar, the cosmic ray production rate is still significant at higher energies. Figure 3 shows the production rate as a function of energy for the cosmic ray flux. Since there is a spectral difference between the 4FP60R flux and the cosmic ray flux above 200 MeV, we must use theory along with our measurements to estimate the cosmic-ray production. Therefore, we must consider the possibility that an energy dependence in the theoretical cross section used for this extrapolation will introduce a systematic uncertainty. The input physics to the CEM03.02 cross sections does not change over the energy range of interest and no known physics is omitted. Therefore one does not expect the

TABLE IX. A summary of the estimates of the uncertainty in the cosmic-ray production rate due to the uncertainty in the energy dependence of the cross-section extrapolation. The second column gives the neutron energy range over which the CEM code predicts the majority of the production rate for the 4FP60R beam spectrum and our isotopic sample. The third column gives the neutron energy range for which the CEM code predicts the majority of the production rate for a cosmic ray beam spectrum and a 86–14% enriched sample. The fourth column gives the fraction of the production rate arising from neutrons with energy less than 200 MeV. The fifth column is the estimated uncertainty in the energy dependence of the cross section as described in the text. The last column provides the deduced uncertainty contribution to the cosmic-ray production rate resulting from scaling our measurements.

Isotope	Critical E_n for beam prod. rate (MeV)	Critical E_n for cosmic prod. (MeV)	Fraction cosmic prod. for $E_n < 200$ MeV (%)	Est. uncertainty in energy dependence of cross section (%)	Deduced uncertainty in production rate (%)
^{57}Co	170–420	280–1040	1.9	50	49
^{54}Mn	200–490	330–1190	1.0	50	50
^{68}Ge	35–250	110–530	44.2	15	8.4
^{65}Zn	110–300	140–640	29.2	35	24.8
^{60}Co	140–350	190–890	12.4	50	43.8

uncertainty for the production of ^{68}Ge. The $\Delta A = 8$ transitions in ^{56}Fe producing nuclei ^{48}Cr, ^{48}V, and ^{48}Sc are then used for this comparison. The ratio of the measured and calculated cross sections for these processes varies by an average of $\approx 15\%$ between 300 and 500 MeV. We estimate the uncertainty in the extrapolation to higher energies as being equal to this 15% variation scaled to the fraction of model-predicted cosmic-ray production above 200 MeV. The result is given in Table IX.

This uncertainty contribution differs for each isotope due to the different critical neutron energy ranges, the different fraction of cosmic-ray production rate over 200 MeV, and the different results of the comparison of theory to data in Ref. [33]. For the $\Delta A = 11$ production of ^{65}Zn, we used the data and theory of the isotope production of ^{44}Sc and ^{44}K between 300 and 750 MeV with the result that the ratio varies $\approx 35\%$. For the $\Delta A = 16$ production of ^{60}Co, we used the data and theory of the isotope production of ^{41}Ar and ^{39}Cl between 300 and 750 MeV with the result that the ratio varies $\approx 50\%$. For the $\Delta A = 19$ production of ^{57}Co, we used the data and theory of the isotope production of ^{38}Cl and ^{38}S between 300 and 1000 MeV with the result that the ratio varies $\approx 50\%$. For the $\Delta A = 22$ production of ^{54}Mn, we used the data and theory of the isotope production of ^{38}Cl and ^{28}Mg between 300 and 1000 MeV with the result that the ratio varies $\approx 50\%$. All these results are summarized in Table IX along with the deduced uncertainty in the estimated cosmic-ray production rate. The uncertainty associated with this scaling dominates the total uncertainty for the cosmic-ray production rate estimates (see Table XI). Because the production rate of ^{68}Ge is concentrated at lower energies, the theoretical extrapolation for this important isotope is more reliable than the others.

A reader may prefer to use a different cross-section model to estimate the production due to cosmic rays. If so, Eqs. (1) and (7) can be used with a different model to interpret our measurements of the production rate at WNR in terms of the cosmic ray flux. Furthermore, the uncertainty assigned to the choice of the cross-section model's energy dependence is not based on neutron projectile data, due to a lack of such data. Therefore, one must recognize the caveat this introduces in the extrapolation of the measured production rate values to predicted cosmic-ray production rates.

V. CONVERTING THE MEASURED PRODUCTION RATES TO COSMOGENIC PRODUCTION RATES

To estimate the production rate due to cosmic-ray neutrons, one must know the energy dependent flux of the neutrons and the cross sections.

Ziegler carried out a comprehensive study on the cosmic-ray neutron flux [25] and pointed out that some of the data from early measurements is incorrect or of marginal quality. Mei *et al.* [21] recognized that previous estimates of the cosmogenic production rates used various outdated estimates of the cosmic neutron flux. Improved recent measurements by Gordon *et al.* [26] show that the flux density spectrum at sea level can be parameterized as

$$\phi(E) = 1.006 \times 10^{-6} e^{-0.35 \ln^2 E + 2.1451 \ln E}$$
$$+ 1.011 \times 10^{-3} e^{-0.4106 \ln^2 E - 0.667 \ln E} \tag{7}$$
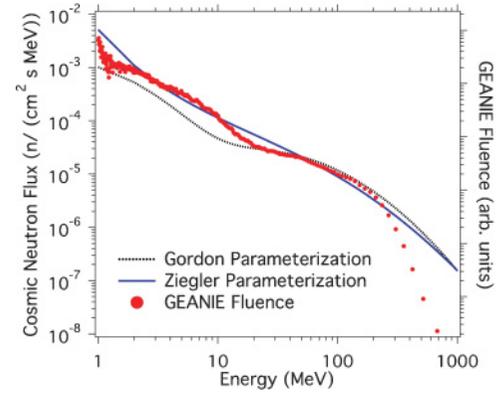
FIG. 4. (Color online) The measured neutron flux parametrization functions at sea level [25,26] and a normalized plot of the 4FP60R neutron fluence showing that the spectral shape in the critical 100- to 300-MeV range is similar to the cosmic ray spectrum.

where E is neutron kinetic energy in MeV and ϕ is given in units of cm^{-2} s^{-1}MeV^{-1}. This parametrization function agrees with the data within $\sim 2\%$. Note that parametrization used by Ref. [16] based on that from Ref. [25] differs from that of Ref. [26]. Both curves are shown in Fig. 4.

Gordon's measurements show that the shape of the outdoor ground-level neutron spectrum does not depend significantly on altitude, cutoff, or solar modulation. Factors depending on atmospheric depth, geomagnetic cutoff, rigidity, and geomagnetic location are given by Gordon for correcting the flux for these effects. His model differs slightly from that of Ziegler or from the JEDEC standard. As a comparison, the cosmic production rates resulting from Gordon's flux are 13–33% higher than that using the flux of Ziegler for the isotopes of interest in this work.

The ratio of N_0 to N_0^{Pred} values given in Table III can be used to scale a predicted production rate (K_{Gordon}) based on the cross sections of Sec. IV and the Gordon neutron flux parametrization to provide an estimate (K_{scaled}) of the cosmogenic production rate indicated by our measurements. The numbers used in this arithmetic are summarized in Table X

TABLE X. A summary of the parameters that enter into the calculation of our estimate for the cosmic-ray production rate of the various isotopes (K_{scaled}). The uncertainties quoted for K_{scaled} are explained in Table XI. The value for ^{57}Co is taken as that of the 122-keV line as it has a much smaller total uncertainty. The ^{60}Co value is the average of the two individual measurements and, since the uncertainty is dominated by systematic effects, we quote the larger of the two associated total uncertainty values given in Table XI. These production rate values are for a nominal 86% ^{76}Ge 14% ^{74}Ge isotopic mixture.

Isotope	Ratio $\left(\frac{N_0}{N_0^{\mathrm{Pred}}}\right)$	K_{Gordon} [atoms/(kg d)]	K_{scaled} [atoms/(kg d)]
^{57}Co	0.25 ± 0.01	2.93	0.72 ± 0.37
^{54}Mn	0.67 ± 0.03	2.91	1.96 ± 1.01
^{68}Ge	0.36 ± 0.03	5.83	2.12 ± 0.39
^{65}Zn	0.55 ± 0.01	16.24	8.94 ± 2.53
^{60}Co	0.63 ± 0.03	4.06	2.55 ± 1.20

TABLE XI. A summary of the uncertainties (in %) that contribute to the total uncertainty of cosmic production rate. The column labeled *Subtotal* refers to the quadrature sum of all non-cosmic-ray-related contributions and provides the uncertainty for the ratio in Table X.

Isotope (line energy)	Counting statistics	Efficiency	Source activity	Predicted 4FP60R fluence	Flux chamber live time	Subtotal	Cosmic neutron flux	Neutron specral difference	Proton correction	Total
^{57}Co(122)	2.9	0.4	1.0	0.9	0.3	3.2	12.5	49	5.0	51
^{57}Co(136)	16.3	1.2	1.0	0.9	0.3	16.4	12.5	49	5.0	53
^{54}Mn	4.0	1.0	1.0	1.2	0.3	4.4	12.5	50	5.0	51
^{68}Ge	9.1	2.4	1.0	0.5	0.3	9.5	12.5	8.4	5.0	18
^{65}Zn	1.1	2.2	1.0	0.5	0.3	2.7	12.5	24.8	5.0	28
^{60}Co(1173)	3.0	3.0	1.0	0.6	0.3	4.5	12.5	44	5.0	46
^{60}Co(1332)	3.2	1.8	1.0	0.6	0.3	3.9	12.5	44	5.0	46

with the results also quoted in Table II for comparison to previous predictions.

The estimate of the cosmogenic production from these measured results have some additional systematic uncertainties. These include the precision to which the cosmic ray neutron flux is known (10–15% and so we split the difference and use 12.5% [26]). The total cosmogenic rate includes contributions from subdominant proton and pion interactions. These only contribute approximately 10% [20] to the total production rate. These charged particles are much less penetrating than neutrons and therefore their impact on any given sample is very geometry dependent. Hence we assume a 50% uncertainly on this correction for an uncertainty of 5%. Again these uncertainties are uncorrelated and result in a estimated systematic uncertainty of 13.5%.

We estimated the rate of cosmogenic production in ^{enr}Ge with isotopic abundance limited to isotopes 74 (14%) and 76 (86%). However, a small admixture of isotope 70 can result in significantly more ^{68}Ge due to the much lower threshold for the neutron reaction and the higher cross section. Here we present a rough formula to estimate the ^{68}Ge production rate (P_{68}) as a function of the amount of ^{70}Ge present in the sample in percentage (X).

$$P_{68} = (2.12 + 0.75X) \text{ atoms}/(\text{kg d}). \quad (8)$$

This formula should be accurate to approximately 20%. The other critical isotope for $\beta\beta$ research is ^{60}Co and it has a small production dependence on the fraction of ^{70}Ge.

VI. DISCUSSION AND CONCLUSION

We measured the production of ^{57}Co, ^{54}Mn, ^{68}Ge, ^{65}Zn, and ^{60}Co in a sample of Ge enriched in isotope 76 due to high-energy neutron interactions within a neutron beam with a spectrum similar to that of the cosmic-ray neutron flux at the Earth's surface. The uncertainty on the beam-produced production rate at those energies is below 10%, depending on isotope, as given in Table XI. The results, presented in Table III,

were compared to cross sections calculated with CEM03.02. The measurements are smaller by about a factor of 2–4 than these calculations depending on isotope. We scaled these measurements using CEM03.02 cross sections to estimate the cosmic-ray production rate of these troublesome isotopes and present the results in Table X. Our estimated total uncertainty for the production rate of the critical ^{68}Ge isotope is approximately 20% providing much better guidance to double β decay experimenters in their efforts to understand background due to this isotope. The uncertainties on the deduced cosmogenic production is dominated by the uncertainty in the extrapolation of the cross sections to higher neutron energies. This large uncertainty arises due to a lack of large ΔA, neutron-induced reactions at higher incident energies with which to validate the theory used for the extrapolation.

[1] S. R. Elliott and P. Vogel, Annu. Rev. Nucl. Part. Sci. **52**, 115 (2002).

[2] S. R. Elliott and J. Engel, J. Phys. G: Nucl. Part. Phys. **30**, R183 (2004).

[3] A. S. Barabash, F. Hubert, P. Huber, and V. I. Umatov, Phys. At. Nucl. **67**, 438 (2004).

[4] F. T. Avignone III, G. S. King III, and Y. Zdesenko, New J. Phys. **7**, 6 (2005).

[5] H. Ejiri, J. Phys. Soc. Jpn. **74**, 2101 (2005).

[6] F. T. Avignone III, S. R. Elliott, and J. Engel, Rev. Mod. Phys. **80**, 481 (2008).

[7] C. E. Aalseth *et al.* (IGEX Collaboration), Phys. Rev. D **65**, 092007 (2002).

[8] L. Baudis *et al.*, Phys. Rev. Lett. **83**, 41 (1999).

[9] H. V. Klapdor-Kleingrothaus and I. V. Krivosheina, Mod. Phys. Lett. A **21**, 1547 (2006).

[10] S. Elliott *et al.*, *Proceedings of the Carolina International Symposium on Neutrino Physics* (IOP, London, 2010), Vol. 173.

[11] V. E. Guiseppe *et al.*, in *Nuclear Science Symposium Conference Record* (2008). NSS'08, IEEE (Dresden, Germany, 2008), pp. 1793–1798, arXiv:0811.2446 [nucl-ex].

[12] R. Henning *et al.* (2009), The 10th Conference on the Intersections of Particle and Nuclear Physics (CIPANP 2009) (to be published), arXiv:0907.1581.

[13] S. Schönert *et al.*, Nucl. Phys. Proc. Suppl. **145**, 242 (2005).

[14] H. S. Miley, F. T. Avignone, R. L. Brodzinski, W. K. Hensley, and J. H. Reeves, Nucl. Phys. B, Proc. Suppl. **28**, 212 (1992).

[15] F. T. Avignone *et al.*, Nucl. Phys. B, Proc. Suppl. **28**, 280 (1992).

[16] S. Cebrián *et al.*, J. Phys.: Conf. Ser. **39**, 344 (2006).

[17] T. Horiguchi *et al.*, Int. J. Appl. Rad. Isot. **34**, 1531 (1983).

[18] Y. V. Aleksandrov *et al.*, Bull. Russ. Acad. Sci.: Phys. Ser. **59**, 895 (1995).

[19] E. B. Norman *et al.*, Nucl. Phys. B, Proc. Suppl. **143**, 508 (2005).

[20] I. Barabanov, S. Belogurov, L. Bezrukov, A. Denisov, V. Kornoukhov, and N. Sobolevsky, Nucl. Instrum. Methods B **251**, 115 (2006).

[21] D.-M. Mei, Z.-B. Yin, and S. R. Elliott, Astropart. Phys. **31**, 417 (2009).

[22] A. Balysh *et al.*, in *Proceedings of the XXVIIth Rencontre de Moriond Progress in Atomic Physics Neutrinos and Gravitation* (Editions Frontieres, Singapore, 1992), p. 177.

[23] J. J. Back and Y. A. Ramachers, Nucl. Instrum. Methods A **586**, 286 (2008).

[24] A. J. Koning, S. Hilaire, and M. C. Duijvestijn, in *Proceedings of the International Conference on Nuclear Data for Science and Technology—ND2004*, edited by R. C. Haight, M. B. Chadwick, T. Kawano, and P. Talou (2004), Vol. 769, p. 1154.

[25] J. F. Ziegler, IBM J. Res. Dev. **42**, 117 (1998).

[26] M. S. Gordon and P. Goldhagen *et al.*, IEEE Trans. Nucl. Sci. **51**, 3427 (2004).

[27] H. V. Klapdor-Kleingrothaus *et al.*, Nucl. Instrum. Methods A **481**, 149 (2002).

[28] P. W. Lisowski, C. D. Bowman, G. J. Russell, and S. A. Wender, Nucl. Sci. Eng. **106**, 208 (1990).

[29] J. A. Becker and R. O. Nelson, Nucl. Phys. News **7**, 11 (1997).

[30] K. K. Gudima, S. G. Mashnik, and V. D. Toneev, Nucl. Phys. A **401**, 329 (1983).

[31] S. G. Mashnik, M. I. Baznat, K. K. Gudima, A. J. Sierk, and R. E. Prael, J. Nucl. Radiochem. Sci. **6**, A1 (2005).

[32] S. G. Mashnik, K. K. Gudima, R. E. Prael, A. J. Sierk, M. I. Baznat, and N. V. Mokhov, LANL Report LA-UR-08-2931, Los Alamos (2008), arXiv:0805.0751, *Invited lectures presented at the Joint ICTP-IAEA Advanced Workshop on Model Codes for Spallation Reactions*, February 4-8, 2008, ICTP, Trieste, Italy.

[33] Yu. E. Titarenko *et al.*, Phys. Rev. C **78**, 034615 (2008).

[34] Y. A. Korovin, A. A. Natalenko, A. Y. Konobeyev, A. Y. Stankovskiy, and S. G. Mashnik, Nucl. Instrum. Methods A **624**, 20 (2010).